JOURNAL OF MATERIALS SCIENCE 19 (1984) 1791–1798

Determination of transient creep parameters for HPSN by dynamic bending tests

T. FETT
Kernforschungszentrum Karlsruhe, Arbeitsgruppe Zuverlässigkeit und Schadenskunde am Institut für Reaktorbauelemente, West Germany

D. MUNZ
Universität Karlsruhe, Institut für Zuverlässigkeit und Schadenskunde im Maschinenbau, West Germany

A procedure is proposed which allows to determine creep parameters, mainly in the transient creep range, by dynamic bending tests. From measurements on HPSN at 1200° C creep exponents in the range $5 < n < 12$ were found. The influence of creep on bending strength is investigated.

1. Introduction

Fracture in bending tests of ceramic materials is caused by flaws introduced during fabrication or surface preparation. In the case of subcritical crack extension before final unstable crack growth, the fracture stress is dependent on the loading rate. By application of linear elastic fracture mechanics it is possible to predict this dependency from the material parameters of subcritical crack extension or to determine these parameters from the measured fracture stress. At high temperatures creep may complicate the fracture behaviour. If the creep parameters for transient creep are known, corrections can be introduced in the linear elastic fracture mechanics relations [1, 2]. In this paper it is shown that these creep parameters can be evaluated from the same dynamic bending tests that have to be performed anyway to obtain the subcritical crack growth parameters.

2. Creep behaviour of HPSN at elevated temperatures

High temperature creep behaviour of ceramic materials can be described by creep curves which are similar to those of most metals. Hot pressed silicon nitride (HPSN) shows typical creep curves under constant load demonstrated by the results of Kossowsky *et al.* [3] and Din and Nicholson [4] (Fig. 1). In the first stage (I) the creep rate decreases from high initial values until a constant creep rate is reached in the steady-state stage (II). Finally, in the third stage (III), the creep rate accelerates producing cracks followed by failure. The third stage will not be found under all test conditions.

Creep curves can be described by an equation proposed by Pao and Marin [5, 6] as the sum of elastic, transient and steady-state components

$$\dot{\epsilon} = \dot{\sigma}/E + a(C\sigma^n - \epsilon') + B\sigma^n \qquad (1)$$

where ϵ' means the transient creep strain accumulated during load application. Since the stress rate is expressed in terms of stress and strain, Equation 1 is called a strain hardening formulation.

For dynamic bending tests in the first region of transient creep where $\epsilon' \ll C\sigma^n$, Equation 1 is simplified to become

$$\dot{\epsilon} \cong \dot{\sigma}/E + D\sigma^n \qquad (2)$$

with $D = aC + B$. In this approach creep rate becomes only dependent on stress.

3. Stress–deformation behaviour under constant strain rate condition

By application of Equation 2 the stress-strain behaviour in the transient stage can be calculated for different cases of deformation. In this chapter the case of a tensile test with constant strain rate $\dot{\epsilon}$ will be examined. First, some abbreviations will be defined

0022–2461/84 $03.00 + .12

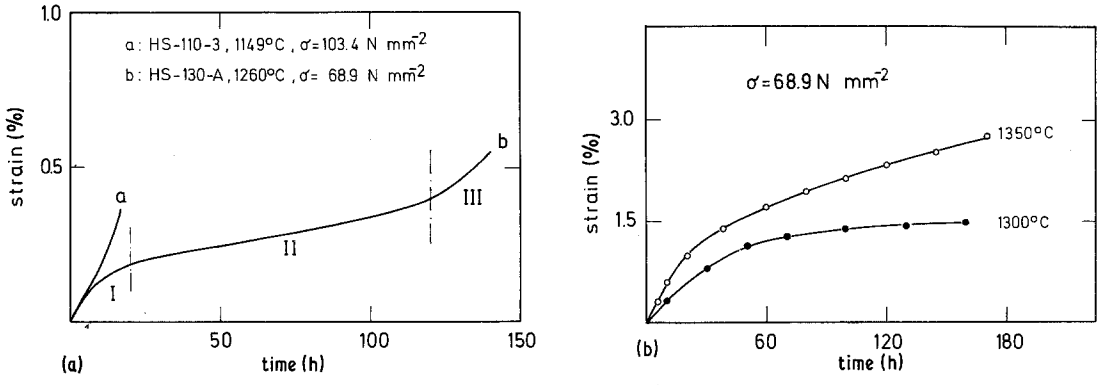

Figure 1 Creep curves of HPSN at elevated temperatures measured by (a) Kossowsky *et al.* [3] and (b) Din and Nicholson [4].

$$u = \sigma/\sigma_\infty \qquad \sigma_\infty = (\dot{\epsilon}/D)^{1/n}$$
$$u_e = \sigma_e/\sigma_\infty \qquad \sigma_e = \dot{\epsilon}Et \tag{3}$$

σ_∞ is an upper boundary value of stress, which would occur, if Equation 2 were valid for unlimited strains and time, respectively. From Equation 2 one obtains an integral representation

$$\int_0^u \frac{du}{1-u^n} = u_e \tag{4}$$

3.1. Analytical solutions for integer n

Equation 4 can be integrated for integer values of n. The first solutions are

$$\sigma = \sigma_\infty[1-\exp(-\sigma_e/\sigma_\infty)] \quad \text{for } n = 1 \tag{5}$$

$$\sigma = \sigma_\infty \tanh(\sigma_e/\sigma_\infty) \quad \text{for } n = 2 \tag{6}$$

$$\frac{1}{6}\ln\frac{1-\sigma/\sigma_\infty}{1+\sigma/\sigma_\infty+(\sigma/\sigma_\infty)^2} + \frac{1}{3^{1/2}}\arctan\frac{2\sigma/\sigma_\infty+1}{3^{1/2}} = \sigma_e/\sigma_\infty \quad \text{for } n = 3 \tag{7}$$

$$\tfrac{1}{2}\operatorname{artanh}(\sigma/\sigma_\infty) + \tfrac{1}{2}\arctan(\sigma/\sigma_\infty) = \sigma_e/\sigma_\infty \quad \text{for } n = 4 \tag{8}$$

$$\sigma/\sigma_\infty = \begin{cases} \sigma_e/\sigma & \text{for } \sigma_e/\sigma_\infty < 1 \\ 1 & \text{for } \sigma_e/\sigma_\infty \geqslant 1 \end{cases} \quad \text{for } n \to \infty \tag{9}$$

For other integers $n > 4$ the solution of Equation 4 can also be expressed by elementary functions [7]. Unfortunately, the solutions are given implicitly if $n > 2$.

The results are shown in Fig. 2. Because of Equation 3, σ_e/σ_∞ stands for time and strain, respectively.

3.2. Approximate solution for the stress–strain behavior in tensile tests

To transfer the $\sigma-\epsilon$ behaviour from tensile tests to bending tests, explicit representation of stresses is necessary. From curves in Fig. 2 we note that the higher the value of n, the later the curve devi-

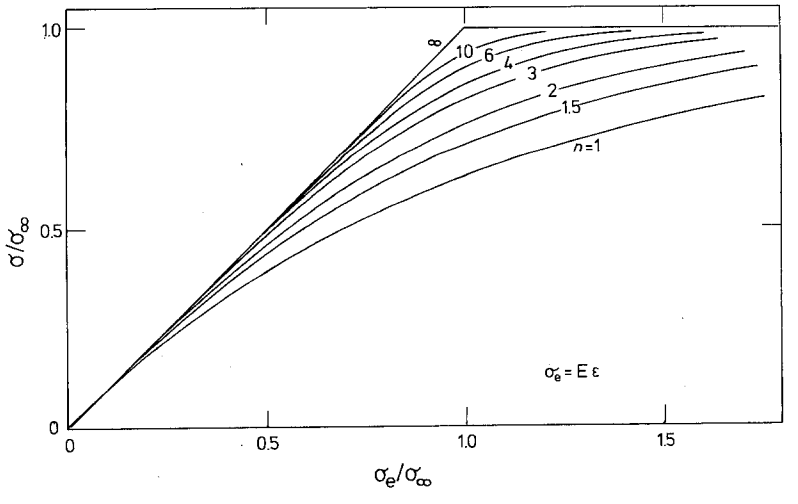

Figure 2 Stress–strain curves in tensile tests, calculated with Equation 4.

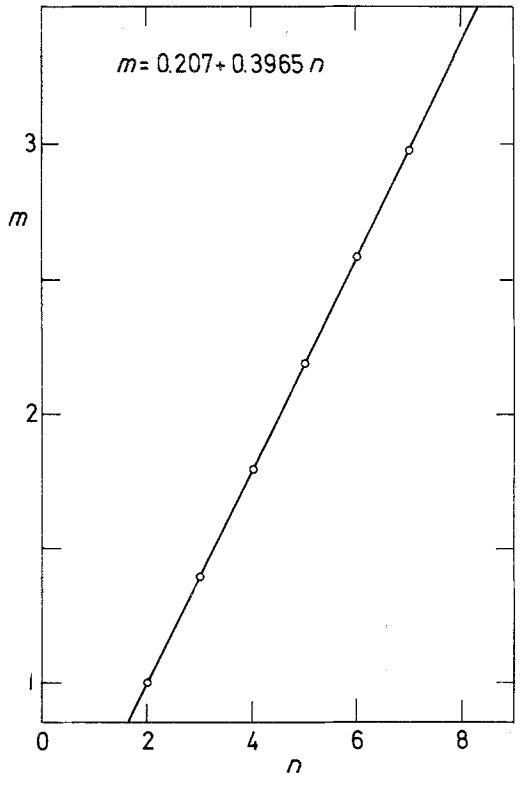

Figure 3 Parameter m as a function of creep exponent n.

ates from the initial straight line. This indicates that an expression

$$\sigma/\sigma_\infty = \tanh^{1/m}(\sigma_e/\sigma_\infty)^m \quad \text{with } m = f(n) \tag{10}$$

should give a good approximation.

The parameter m was determined under the condition, that the approximation and exact solution was identical for $\sigma_e/\sigma_\infty = 1$. The relation between m and n is depicted in Fig. 3 and can be expressed by

$$m = 0.207 + 0.3965n \tag{11}$$

The maximum inaccuracy of Equations 10 and 11 is better than ± 1% in the range $1.5 \leqslant n \leqslant 15$. In case of $n = 2$, Equation 10 is exact.

4. Bending moment in dynamic bending tests

In dynamic bending tests the reaction of the deformed bar is given by the bending moment M. In case of symmetrically distributed stresses M is given by

$$M = 2b\int_0^{h/2} \sigma(x)x\mathrm{d}x \tag{12}$$

where b is the thickness and h is the height of the specimen, and x is the distance from the neutral axis.

By application of the hypothesis of Bernoulli that plane cross-sections will remain plane during bending deformations, we get

$$\begin{aligned} \epsilon(x) &= \epsilon(1)2x/h \\ \sigma_e(x) &= \sigma_e(1)2x/h \qquad \sigma_e(1) = \epsilon(1)E \\ \sigma_\infty(x) &= \sigma_\infty(1)(2x/h)^{1/n} \quad \sigma_\infty(1) = (\dot{\epsilon}(1)/D)^{1/n} \end{aligned} \tag{13}$$

The bracket (1) stands for $2x/h = 1$, i.e. for the outer fibre. Analytical solutions of Equation 12 can be obtained for $n = 1$ and $n \to \infty$.

4.1. Case $n = 1$

Introducing Equations 5 and 13 in Equation 12 leads to

$$M = \tfrac{1}{6}bh^2\sigma_\infty(1)\{1 - \exp[-\sigma_e(1)/\sigma_\infty(1)]\} \tag{14}$$

and asymptotically, if $\sigma_e(1) \to \infty$

$$M_\infty = \tfrac{1}{6}bh^2\sigma_\infty(1) = W\sigma_\infty(1) \tag{15}$$

Thus it yields

$$\begin{aligned} M/M_\infty &= 1 - \exp(-M_e/M_\infty) \\ M_e &= \sigma_e(1)W \end{aligned} \tag{16}$$

4.2. Case $n \to \infty$

In this special case the stress–strain relation is given by Equation 9. The accompanying bending moment becomes

$$M/2b = \int_0^{x'} \sigma_e x\mathrm{d}x + \int_{x'}^{h/2} \sigma_\infty x\mathrm{d}x \tag{17}$$

with

$$x' = \frac{\sigma_\infty}{\sigma_e(1)}h/2$$

The integration yields

$$M/2b = \tfrac{1}{8}\sigma_\infty h^2 - \tfrac{1}{24}\sigma_\infty^3 h^2/\sigma_e(1)^2 \tag{18}$$

$$M_\infty = \tfrac{1}{4}\sigma_\infty h^2 b = \tfrac{3}{2}\sigma_\infty W \tag{19}$$

with the result

$$\begin{aligned} \frac{M}{M_\infty} &= 1 - \tfrac{4}{27}(M_\infty/M_e)^2 \quad \text{for } M_e/M_\infty > 2/3 \\ \frac{M}{M_\infty} &= \frac{M_e}{M_\infty} \qquad\qquad\qquad \text{for } M_e/M_\infty \leqslant 2/3 \end{aligned} \tag{20}$$

4.3. General case $1 < n < \infty$

The general case $1 < n$ can be treated by appli-

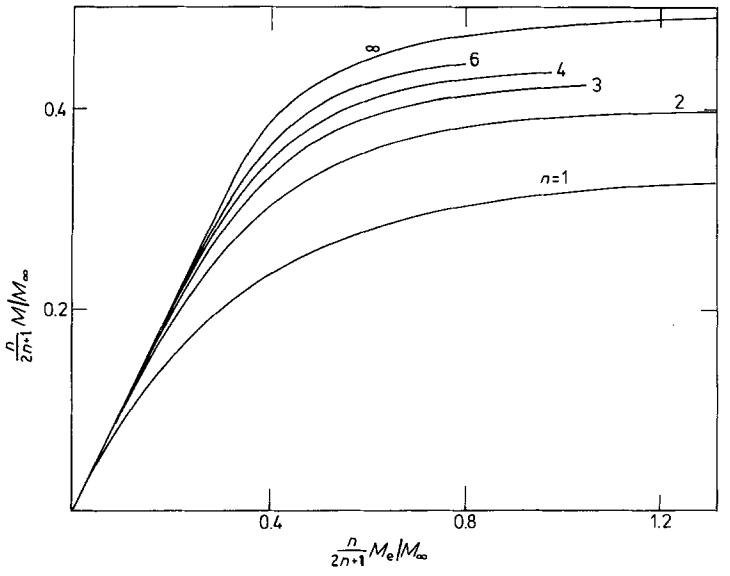

Figure 4 Bending moments in dynamic bending tests, calculated with Equations 16, 20 and 22.

cation of Equation 10. Substitution of Equations 10 and 13 into Equation 12 gives

$$M = 3W\sigma_\infty(1) \times \int_0^1 y^{(n+1)/n} \{\tanh [\sigma_e(1)/\sigma_\infty(1) y^{(n-1)/n}]^m\}^{1/m} dy$$

with $y = 2x/h$.

At high outer fibre strains an upper boundary value of the bending moment appears

$$M_\infty = W \frac{3n}{2n+1} \sigma_\infty(1) \qquad (21)$$

and with this relationship it follows

$$\frac{M}{M_\infty} = \frac{2n+1}{n} \int_0^1 y^{(n+1)/n} \left\{ \tanh \left[\frac{3n}{2n+1} \times \frac{M_e}{M_\infty} y^{(n-1)/n} \right]^m \right\}^{1/m} dy \qquad (22)$$

This definite integral cannot be solved in a closed manner, so it was evaluated numerically.

In Fig. 4 the result is represented in a normalized form

$$\frac{n}{2n+1} M/M_\infty = f\left(\frac{n}{2n+1} M_e/M_\infty \right) \qquad (23)$$

for several values of n.

5. Procedure for estimation of creep parameters from bending-moment–deflection curves

From each bending test usually a bending-moment against deflection curve (at least a bending-moment against time curve) is recorded. Therefore, it can be shown how the creep parameters n and $\sigma_\infty(1)$ can be determined without requiring additional tests.

5.1. Determination of n

Three curves from Fig. 4 are shown once more in Fig. 5. Two straight lines with 95% and 90% of

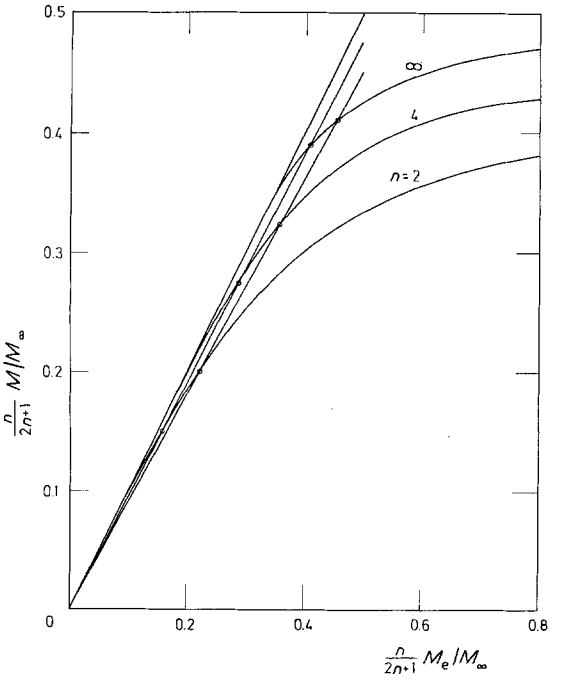

Figure 5 Procedure for determination of creep exponent n from the shape of bending moment against deflection curves.

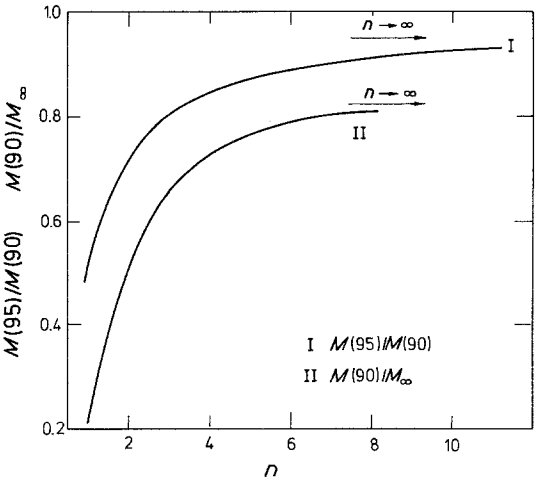

Figure 6 Bending moment ratios as a function of n.

initial slope are drawn in this diagram. For each value of n the bending moments at the points of intersection $M(95\%)$ and $M(90\%)$ are determined and the quotient $M(95\%)/M(90\%)$ is calculated. In Fig. 6 this quotient is plotted against n.

The dependence $n = f[M(95\%)/M(90\%)]$ can be expressed by a polynomial

$$1/n = a_0 + a_1X + a_2X^2 + a_3X^3 + a_4X^4 \quad (24)$$

where $X = 0.948 - M(95\%)/M(90\%)$ for $X \geqslant 0.015$ with the coefficients

$$a_0 = 0.05858 \quad a_1 = 1.7756 \quad a_2 = 1.2182$$

$$a_3 = -4.9715 \quad a_4 = 9.3219$$

5.2. Determination of M_∞, $\sigma_\infty(1)$

Because of Equation 21 the parameters M_∞ and $\sigma_\infty(1)$ are equivalent and related to the creep parameter D (Equation 3). For the determination of M_∞ an analogous procedure is suggested. In Fig. 6 the calculated quotients $M(90\%)/M_\infty$ are plotted against n.

In the range $1 \leqslant n \leqslant 20$ the resulting curve can be given by

$$\frac{M(90\%)}{M_\infty} = \frac{2n+1}{n}(b_0 + b_1/n + b_2/n^2 + b_3/n^3 + b_4/n^4) \quad (25)$$

with

$$b_0 = 0.824 \quad b_1 = -0.1545 \quad b_2 = -3.1984$$

$$b_3 = 4.653 \quad b_4 = -1.981$$

From an experimental bending moment against time curve the intersection with a 90% straight line is stated. Since n is known, the quotient $M(90\%)/M_\infty$ can be taken from Fig. 6 or Equation 25 and the corresponding M_∞ is determined. Because of Equation 21, $\sigma_\infty(1)$ is also known.

6. Measurement on HPSN at 1200° C

Experiments were performed with hot pressed silicon nitride* containing 2.5 wt% MgO and with a density of 3.20 g cm^{-3}. Specimens of 3.5 mm x 3.5 mm x 45 mm were diamond machined from plain parallel billets and annealed in a vacuum of 10^{-5} torr for 4 h at 1200° C.

6.1. Determination of the creep parameters

Dynamic four-point bending tests (20 mm inner, 40 mm outer span) were conducted at 1200° C in a furnace with constant crosshead rates. Bending moment against time and against deflection diagrams were recorded. From the load–time records an initial outer fibre stress rate $\dot{\sigma}_e(1)$ was calculated on the assumption of elastic stress distribution in the cross-section. Fig. 7 shows a diagram recorded with a crosshead speed of $v = 0.025$ mm min^{-1}. The analysis gives $M(95\%) = 2800$ N mm and $M(90\%) = 3090$ N mm. With Equation 24 we find $n \simeq 7$ and from Equation 25 we obtain $M(90\%)/M_\infty = 0.805 \rightarrow M_\infty = 3838$ N mm.

By application of Equation 21 we obtain $\sigma_\infty(1) = 293.3$ N mm^{-2} at the stress rate $\dot{\sigma}_e(1) = 0.94$ N mm^2 sec^{-1}. The diagrams of four single tests with nearly equal values $n = 7$ are plotted point by point in a common diagram (Fig. 8). In addition, the dash-dotted line represents the dependence calculated with Equation 22. A good agreement between measurement and calculation is found.

A greater number of bending tests lead to a range of $6 \leqslant n < 12$. Fig. 9 shows the diagram with the maximum value found of $n = 11.9$. The calculated normalized bending moment M/M_∞ is plotted point by point and gives also a good agreement.

To analyse the stress deformation behaviour – for instance by Equation 1 – the combination ED is of interest. It can be determined by Equation 3

$$ED = \dot{\sigma}_e/\sigma_\infty^n$$

The results of Fig. 8 give a range of

$$ED \approx 0.5\text{–}1.0 \times 10^{-17}\,\text{N}^{-6}\,\text{mm}^{12}\,\text{sec}^{-1}$$

*Ceranox NH 206, Annawerk GmbH, Rödental, Germany.

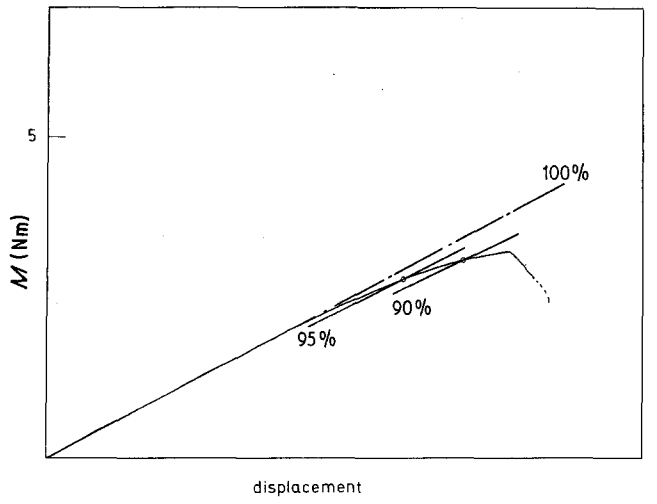

Figure 7 Analysis of an experimentally obtained record (crosshead rate $v = 0.025$ mm min^{-1}).

The Young's modulus at 1200° C measured by sonic resonance [3] is $E \approx 280\,\mathrm{GN\,m^{-2}}$, and so it follows

$$D \approx 1.8\text{–}3.6 \times 10^{-23}\,\mathrm{N^{-2}\,mm^{14}\,sec^{-1}}$$

6.1.1. Comparison with the literature

In this investigation creep exponents $n > 5$ were obtained at 1200° C. These values are mainly caused by transient creep. The data in literature are mostly restricted to the steady-state creep behaviour.

In the case of low bending stresses values in the range $1 < n < 3$ are often reported [3, 4, 8, 9]. Arons and Tien [10] obtained values $3.5 < n < 5.5$. At high stresses – that are necessarily reached in bending strength tests – distinctly higher values of n were found. Measurements of Kossowsky *et al.* [3] gave at 1160° C $n = 2.2$ for $\sigma < 100\,\mathrm{N\,mm^{-2}}$ and $n \approx 50$ for $\sigma > 100\,\mathrm{N\,mm^{-2}}$. It should not be attempted to interpret such high exponents by simple physical models.

6.2. Measurement of bending strength at 1200° C

Measurements of bending strength were carried out with different crosshead rates. The evaluation was done in two ways. The "conventional" bending strength σ_f^* was calculated by use of the well-known formula

$$\sigma_f^* = M_f/W \qquad W = bh^2/6 \qquad (26)$$

where M_f means the bending moment at failure.

The values of σ_f^* are shown in Fig. 10 by open circles. The conventional bending strength is a correct value if creep can be neglected. If the deflec-

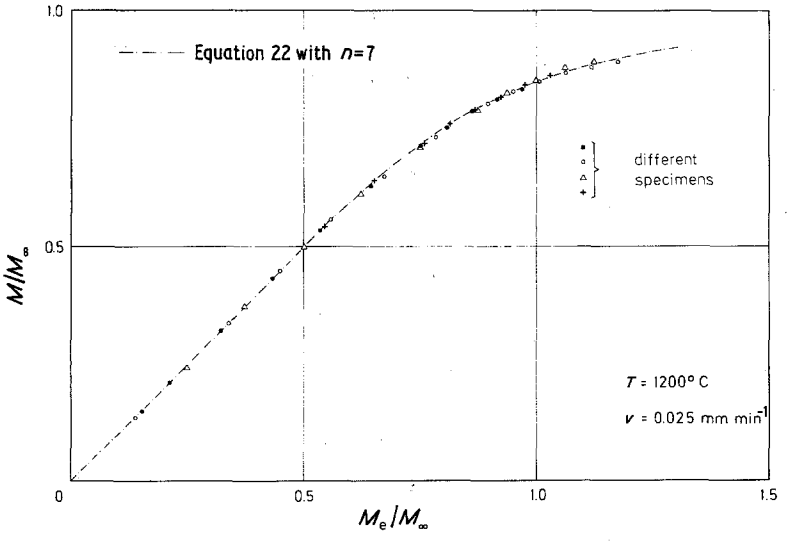

Figure 8 Comparison between calculated and measured bending moment curves.

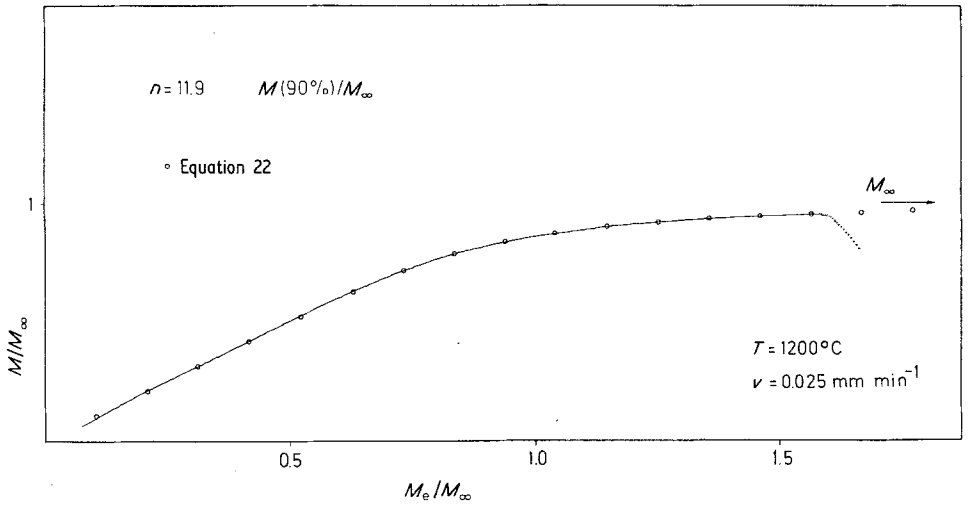

Figure 9 Comparison between measured and calculated bending moment curves for $n = 11.9$.

tion rates are very low, deviations from linearity have to be taken into account. Instead of Equation 26, the more realistic outer fibre stress at the moment of failure $\sigma_f(1)$ should be used.

Outer fibre stresses $\sigma_f(1)$, calculated with Equation 10, are depicted in Fig. 10. The straight line drawn in addition represents the stress $\sigma_\infty(1)$. It constitutes an upper limit for bending strength $\sigma_f(1)$; since Equation (10)

$$\sigma_f(1) \leqslant \sigma_\infty(1)$$

must always be fulfilled. A comparison between $\sigma_f(1)$ and $\sigma_\infty(1)$ is given in [2].

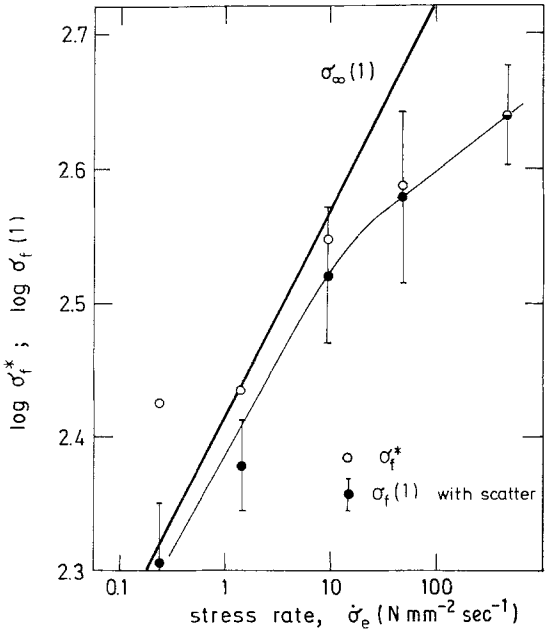

Figure 10 Bending strength of HPSN at 1200° C as a function of stress rate.

7. Conclusion

Dynamic bending tests at high temperatures can be evaluated in such a way that the transient creep parameters can be determined as well as the parameters of subcritical crack extension. This is illustrated in Fig. 11.

(a) From the conventional bending strength σ_f^* the true outer fibre stress at failure $\sigma_f(1)$ can be calculated (Fig. 11a).

(b) In the case of very low deflection rates the strength behaviour is governed by creep effects. From the asymptotic straight line in Fig. 11b the creep parameters n and D are obtained. Using Equations 3 and 10 the approximated relation

$$\sigma_f(1) \to \sigma_\infty(1) \propto \dot{\sigma}^{1/n}$$

is fulfilled.

(c) At high deflection rates, associated with linear load–deflection curves, the influence of creep will vanish, which leads to

$$\sigma_f^* = \sigma_f(1)$$

The asymptotic straight line shows the well-known interdependency of strength and stress rates [11]

$$\sigma_f(1) \propto \dot{\sigma}^{1/(N+1)}$$

caused by subcritical crack growth, N being the crack growth exponent.

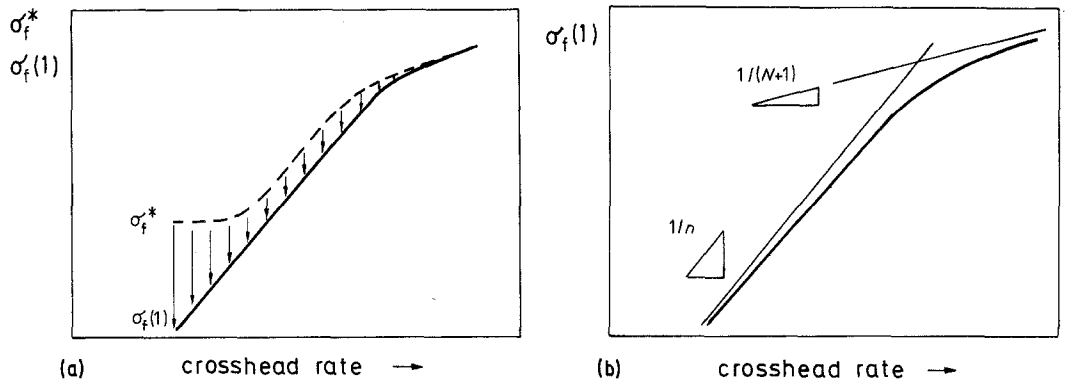

Figure 11 Influence of creep behaviour and subcritical crack growth on true outer fibre stress at failure in dynamic bending tests (schematically).

Acknowledgement

This work was supported by the Deutsche Forschungsgemeinshaft (DFG).

References

1. T. FETT and D. MUNZ, ASTM Symposium on Methods for Assessing the Structural Reliability of Brittle Materials, San Francisco, December 1982. To appear in ASTM-STP 844.
2. T. FETT, Thesis, University of Karlsruhe, 1983 and DFVLR-Forschungsbericht FB 83-07, Deutsche Forschungs- und Versuchsanstalt für Luft- und Raumfahrt, Köln, FR Germany.
3. R. KOSSOWSKY, D. G. MILLER and E. S. DIAZ, *J. Mater. Sci.* **10** (1975), 983.
4. SALAH ud DIN and P. S. NICHOLSON, *ibid.* **10** (1975) 1375.
5. Y. H. PAO and J. MARIN, *J. Appl. Mech.* **20** (1953) 245 ff.
6. I. FINNIE and W. R. HELLER, "Creep of Engineering Materials" (McGraw-Hill Book Comp., New York, 1959).
7. GRÖBNER, HOFREITER; Integraltafeln, Teil II. 4. Auflage, Wien (1965).
8. W. GEBHARD, "Die Ermittlung der Warmfestigkeit keramischer Werkstoffe", DFVLR-Mitt. 81-03, Cologne (1981).
9. F. THÜMMLER and G. GRATHWOHL, "Creep of ceramic materials for gas turbine application", AGARD Report No. 651 (1976) pp. 1–26.
10. R. M. ARONS and J. K. TIEN, *J. Mater. Sci.* **15** (1980) 2046.
11. R. J. CHARLES, *J. Appl. Phys.* **29** (1958) 1657.

Received 19 August
and accepted 13 September 1983